

The molecular gas content of ULIRG type 2 quasars at $z < 1^*$ (Research Note)

M. I. Rodríguez¹, M. Villar-Martín², B. Emonts², and A. Humphrey³
G. Drouart⁴, S. García Burillo⁵, M. Pérez Torres¹

¹ Instituto de Astrofísica de Andalucía (CSIC), Glorieta de la Astronomía s/n, Granada, Spain, e-mail: mrm@iaa.es

² Centro de Astrobiología (INTA-CSIC), Carretera de Ajalvir, km 4, 28850 Torrejón de Ardoz, Madrid, Spain

³ Centro de Astrofísica, Universidade do Porto, Rua das Estrelas, 4150-762 Porto, Portugal

⁴ Dept. of Earth and Space Science, Onsala Space Observatory, Chalmers U. of Technology, SE-43992 Onsala, Sweden

⁵ Observatorio Astronómico Nacional (OAN)-Observatorio de Madrid, Alfonso XII, 3, 28014, Madrid, Spain

November 2013

ABSTRACT

We present new results of CO(1-0) spectroscopic observations of 4 SDSS type 2 quasars (QSO2) at $z \sim 0.3$, observed with the 30m IRAM telescope. The QSO2 have infrared luminosities in the ULIRG (UltraLuminous Infrared Galaxies) regime. We confirm the CO(1-0) detection in one of our 4 QSO2, SDSS J1543-00, with L'_{CO} and M_{H_2} $(1.2 \pm 0.2) \times 10^{10}$ K km s⁻¹ pc² and $(9.4 \pm 1.4) \times 10^9$ M_⊙, respectively. The CO(1-0) line has $FWHM = 575 \pm 102$ km s⁻¹. No CO(1-0) emission is detected in SDSS J0903+02, SDSS J1337-01, SDSS J1520-01 above 3 sigma, yielding upper limits on $M(H_2) \sim 9.6, 4.3$ and 5.1×10^9 M_⊙ respectively. Together with CO measurements of 9 QSO2 at $z \sim 0.3-1.0$ from the ULIRG sample by Combes et al. (2011, 2013), we expand previous studies of the molecular gas content of intermediate z QSO2 into the ULIRG regime. We discuss the location of the 13 ULIRG QSO2 at $z < 1$ with available L'_{CO} measurements in the L'_{CO} vs. z and L'_{CO} vs. L_{FIR} diagrams, in comparison with other QSO1 and ULIRG star forming samples.

Key words. (galaxies:) quasars: general; (galaxies:) quasars: emission lines; galaxies: ISM

1. Introduction

Following the discovery in large numbers of type 2 quasars (QSO2) during the last decade, an intensive follow up has been performed at different wavelengths: X-ray, radio, infrared and optical (e.g., Szokoly et al. 2004, Lacy et al. 2007, Martínez-Sansigre et al. 2006, Zakamska et al. 2003). In spite of this, the molecular gas content of this class of objects has been very scarcely studied.

The study of the molecular gas content in these objects is crucial to better understand the conditions required to trigger both the nuclear and star formation activities in the most luminous active galaxies (AGN), since this gaseous phase can provide large amounts of fuel to form stars and feed the nuclear black hole. It can also provide information about the relation between QSO2 and other systems such as type 1 quasars (QSO1), luminous (LIRG, $10^{11} L_{\odot} \leq L_{IR} < 10^{12} L_{\odot}$) and ultra-luminous (ULIRG, $L_{IR} \geq 10^{12} L_{\odot}$) infrared galaxies, where L_{IR} is the total infrared luminosity ($\sim 8-1000 \mu m$ range). However, only few molecular gas studies of QSO2 have been carried out, and frequently focussed on $z > 2$ objects (see Villar Martín et al. 2013 (VM13 hereafter) and references therein).

2. QSO2 sample at $z < 1$

There are L'_{CO} measurements for 29 QSO2 at $z < 1$ published in three different works. 15 CO(1-0) confirmed detections are reported (i.e. 52% detection rate) which imply molecular gas masses $M(H_2) = \alpha \times L'_{CO}$ in the range $(0.5-15) \times 10^9$ M_⊙¹.

Krips, Neri & Cox (2012, KNC12 hereafter) investigated the molecular gas content of 10 QSO2 at $z \sim 0.1-0.4$ based on observations performed with the IRAM Plateau de Bure Interferometer (PdBI). All but two objects (selected from Zakamska et al. 2003), are from the original sample of 24 μm selected galaxies observed with the Spitzer infrared spectrograph for the 5 millijansky Unbiased Spitzer Extragalactic Survey (5MUSES) (Wu et al. 2010, see also Lacy et al. 2007). KNC12 confirm the detection of CO(1-0) in five sources and a tentative detection for a sixth. The molecular gas masses were found in the range of $M(H_2) \sim (0.4-2.6) \times 10^9$ M_⊙ for the detections and upper limits are in the range $(0.4-2.2) \times 10^9$ M_⊙ for the non detections.

In VM13 we presented the results of CO(1-0) spectroscopic observations of 10 QSO2 at $z \sim 0.2-0.34$ performed with the 30m IRAM radiotelescope and the Australia Telescope Compact Array. All objects were selected from the original sample of QSO2 at $0.3 \lesssim z \lesssim 0.8$ identified by Zakamska et al. (2003) from the Sloan Digital Sky Survey

* Based on observations carried out with the IRAM 30m radiotelescope.

¹ For coherence with other works, we assume $\alpha = 0.8$ M_⊙ (K km s⁻¹ pc²)⁻¹ (Downes & Solomon 1998). Recent results suggest $\alpha = 0.6 \pm 0.2$ (Papadopoulos et al. 2012).

(SDSS, York et al. 2000). 5 new confirmed CO(1-0) detections were reported, with $M(\text{H}_2) \sim (5-6) \times 10^9 M_\odot$, and 1 tentative detection. Upper limits are in the range $(1.6-5.0) \times 10^9 M_\odot$ for the non detections.

Most of these 20 QSO2 (17/20) have $L_{\text{IR}} < 10^{12} L_\odot$, i.e., in the LIRG regime or below. Only three have $L_{\text{IR}} \sim 10^{12} L_\odot$ in the transition between the LIRG and ULIRG regimes. The implied molecular gas masses are found to be consistent with QSO1 of similar infrared luminosities.

Here we expand our work into the ULIRG regime. On one hand, we include results of CO(1-0) observations of 4 ULIRG SDSS QSO2 at $z \sim 0.3$ (Table 1), to match in z the sample by VM13.

We also include 9 objects in the $z \lesssim 1$ ULIRG samples by Combes et al. (2011, 2013; C11 and C13 hereafter). Making use of the original SDSS spectra when available or optical line luminosities published in the literature, we find that the following ULIRG can be classified as QSO2 according to Zakamska et al. (2003) criteria: G19, G30, S1, S4, S8, S10, S12, S21, S25 (the nomenclature in C11, C13 is used). These 9 QSO2 are at $z \sim 0.3-0.9$. Spectroscopic observations of different CO transitions performed with the IRAM 30m radiotelescope imply $M(\text{H}_2) \sim (3.2-15.4) \times 10^9 M_\odot$ for the 5 detections and upper limits $\sim (1.1-7.2) \times 10^9 M_\odot$ for the 4 non detections (C11, C13).

We assume $\Omega_\Lambda = 0.7$, $\Omega_M = 0.3$, $H_0 = 71 \text{ km s}^{-1} \text{ Mpc}^{-1}$.

3. Observations and data reduction

The observations were carried out using the 30m IRAM single dish telescope at Pico Veleta, during two different observing runs in February and June 2013 (programme 202-12). The EMIR receiver was tuned to the redshifted frequencies of the CO(1-0) line (115.27 GHz rest frame), using the optical SDSS z for each object (see Table 1). The observations were performed in the wobbler-switching mode with a throw 50" in order to ensure flat baselines. We observe both polarizations (H and V) using as a backend the WILMA autocorrelator that produced an effective total bandwidth of 4 GHz with a (Hanning-smoothed) velocity resolution of 16 MHz $\sim 50 \text{ km s}^{-1}$. The corresponding T_{sys} , total integration time and the rms corresponding for each source is specified in Table 1. The temperature scale used is in main beam temperature T_{mb} . At 3mm the telescope half-power beam width is $29''$. The main-beam efficiency is $\eta_{\text{mb}} = T_A^*/T_{\text{mb}} = 0.81$ and the conversion factor is $S/T_A^* = 5.9 \text{ Jy/K}$.

The pointing model was checked against bright, nearby calibrators for every source, and every 1.6 hrs for long integrations. It was found to be accurate within $5''$. Calibration scans on the standard two load system were taken every 8 minutes.

The off-line data reduction was done with the CLASS program of the GILDAS software package (Guilloteau & Forveille 1989), and involved only the subtraction of (flat) baselines from individual integrations and the averaging of the total spectra (Fig. 1).

4. Results

4.1. Infrared luminosities

The 4 QSO2 in our sample have an IRAS counterpart at 60 and/or 100 μm , that we have used to constrain the far

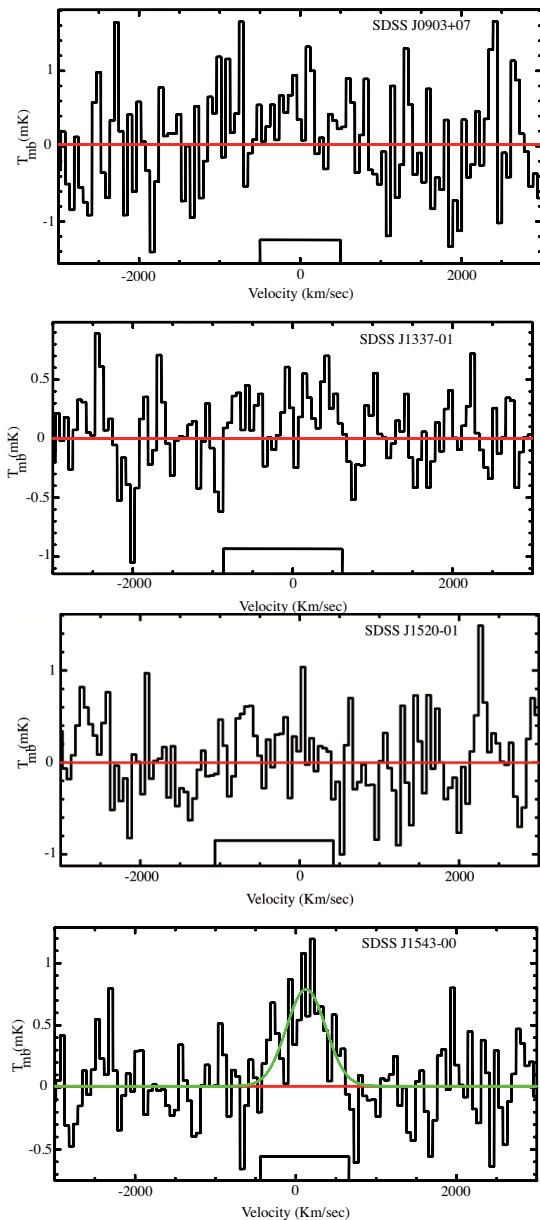


Fig. 1. CO(1-0) spectra of the 4 QSO2 in our sample. The zero velocity corresponds to z_{SDSS} . A fit of the line profile is shown in green for the object with detected emission. The vertical axis shows the corrected-beam temperature. The bottom box represents the velocity window where the line is expected.

infrared luminosities L_{FIR} . For coherence with numerous works published in the literature, we estimate L_{FIR} in the 40-500 μm range applying $F_{\text{FIR}} = 1.26 \times 10^{-11} [2.58 f_{60} + f_{100}] \text{ erg s}^{-1} \text{ cm}^{-2}$ and $L_{\text{FIR}} = 4\pi D_L^2 C F_{\text{FIR}}$, where we assume $C = 1.42$ (Mirabel & Sanders 1996). f_{60} and f_{100} are the IRAS flux densities at 60 and 100 μm in Jy. Although the formula was derived for star forming galaxies at $z = 0$, it is often used also for AGN and galaxies at higher z . Thus, here we consider it adequate for the purpose of comparison with other works (e.g. C11, C13, Bertram et al. 2007).

Measurements in both the 60 and 100 μm bands exist only for SDSS J0903+02, while IRAS detections are reported only in one of the bands for the other 3 QSO2. In such cases, we have constrained the flux in the missing band by assuming typical values of $Q = f_{60\mu\text{m}}/f_{100\mu\text{m}}$ for sim-

Table 1. The sample. z_{SDSS} is the optical redshift derived from the [O III] $\lambda 5007$ line using the SDSS spectra. D_L is the luminosity distance in Mpc. t_{exp} gives the total exposure time per source including calibrations. ν_{obs} is the observed frequency of the CO(1-0) transition and rms is the noise determined from channels with 16 MHz (~ 50 km s $^{-1}$) spectral resolution in mK.

Object	RA(2000)	Dec(2000)	z_{SDSS}	D_L Mpc	t_{exp} hr	ν_{obs} GHz	T_{sys} K	rms mK
SDSS J0903+02	09:03:07.84	+02:11:52.2	0.3290	1716	2.6	86.74	101	0.60
SDSS J1337-01	13:37:35.02	-01:28:15.7	0.3282	1711	5.5	86.79	88	0.27
SDSS J1520-01	15:20:19.75	-01:36:11.2	0.3070	1583	4.4	88.20	93	0.39
SDSS J1543-00	15:43:37.82	-00:44:19.9	0.3107	1605	7.1	87.95	91	0.25

Table 2. The luminosity (2) of the [OIII] $\lambda 5007$ line (Zakamska et al. 2003) is given in logarithmic units of L_{\odot} . L'_{CO} (3) is in units of $\times 10^9$ K km s $^{-1}$ pc 2 , where the upper limits correspond to 3σ . A conversion factor $\alpha = 0.8 M_{\odot} (\text{K km s}^{-1} \text{ pc}^2)^{-1}$ has been assumed to calculate the molecular gas mass (4), with $M(H_2) = \alpha \times L'_{\text{CO}}$. $V_{\text{CO-[OIII]}}$ is the velocity redshift of the CO(1-0) line relative to z_{SDSS} . Columns (8) and (9) give the total infrared (~ 8 -1000 μm) and far infrared (~ 40 -500 μm) IRAS fluxes in mJy, while the luminosities are shown in (10) and (11) in units of $\times 10^{12} L_{\odot}$.

Object	log[OIII]	L'_{CO} $\times 10^9$	$M(H_2)$ $\times 10^9 M_{\odot}$	FWHM_{CO} km s $^{-1}$	$V_{\text{CO-[OIII]}}$ km s $^{-1}$	$F_{60\mu\text{m}}$ mJy	$F_{100\mu\text{m}}$ mJy	L_{FIR} $\times 10^{12} L_{\odot}$	L_{IR} $\times 10^{12} L_{\odot}$
(1)	(2)	(3)	(4)	(5)	(6)	(7)	(8)	(10)	(11)
SDSS J0903+02	8.42	< 12.0	< 9.6	-	-	390	540	2.5	3.8
SDSS J1337-01	8.72	< 5.3	< 4.3	-	-	140	N/A	$1.4^{+0.8}_{-0.3}$	$2.1^{+1.2}_{-0.45}$
SDSS J1520-01	8.29	< 6.8	< 5.4	-	-	N/A	490	$1.2^{+0.3}_{-0.3}$	$1.8^{+0.45}_{-0.4}$
SDSS J1543-00	8.40	11.7 ± 1.8	9.4 ± 1.4	575 ± 102	128 ± 47	130	N/A	$1.1^{+0.7}_{-0.2}$	$1.65^{+1.1}_{-0.3}$

ilar objects. There are 12 SDSS QSO2 at $z \sim 0.3$ -0.4 with IRAS measurements in both bands (Zakamska et al. 2004). These show Q median, average and standard deviation values 0.26, 0.29 and 0.17 respectively. 10/12 (83%) of these QSO2 have Q in the range 0.29 ± 0.15 . The most probable L_{FIR} values and their uncertainties for SDSS J1337-01, SDSS J1520-01 and SDSS J1543-00 have been calculated by using $Q = 0.29 \pm 0.15$. Following VM13, L_{IR} was then constrained by assuming a typical $\xi = \frac{L_{\text{IR}}}{L_{\text{FIR}}} = 1.5$. The results are shown in Table 2. The errors reflect the uncertainty on the range of possible Q values. The 4 QSO2 have L_{IR} in the ULIRG regime ($> 10^{12} L_{\odot}$).

4.2. L'_{CO} and $M(H_2)$

CO(1-0) detection is confirmed in one object (SDSS J1543-00) with $L'_{\text{CO}} = (1.2 \pm 0.2) \times 10^{10}$ K km s $^{-1}$ pc 2 (Table 2). HST images of this quasar show that it is undergoing a major merger event (Villar Martín et al. 2012). Assuming $\alpha = 0.8 M_{\odot} (\text{K km s}^{-1} \text{ pc}^2)^{-1}$, the implied molecular gas mass is $(9.6 \pm 1.6) \times 10^9 M_{\odot}$, which is consistent with molecular gas content of other systems with similar L_{IR} . A 1-Gaussian fit of the line profile implies $\text{FWHM}_{\text{CO}} = 576 \pm 102$ km s $^{-1}$ with a velocity redshift relative [OIII] $\lambda 5007$ of 128 ± 47 km s $^{-1}$. No CO(1-0) is detected in the other 3 QSO2. Following the same procedure described in VM13, 3σ upper limits on the molecular gas masses are estimated to be 9.6, 4.3 and $5.4 \times 10^9 M_{\odot}$ for SDSS J0903+02, SDSS J1337-01, SDSS J1520-01 respectively.

The location of the 4 objects in the L'_{CO} vs. z and L'_{CO} vs. L_{FIR} and diagrams is shown in Fig. 2 as red hollow circles (see VM13 for a detailed discussion), together with other QSO1 (blue symbols) and QSO2 (green symbols) samples (left panels) and star forming ULIRGs at $z < 1$ (right panel). The 9 ULIRG QSO2 from C11 and C13 are represented with green solid squares. These 13 ULIRG QSO2 at $z < 1$ fall on the L'_{CO} vs. L_{FIR} correlation defined by other quasar samples at different z and overlap with the location of star forming ULIRG. L_{FIR} is likely to

be dominated by the starburst contribution in those QSO2 with total $L_{\text{IR}} < 2 \times 10^{12} L_{\odot}$. This is less certain at higher luminosities, where an increasing relative contribution of the AGN might occur (Nardini et al. 2010). Indeed, several QSO2 and QSO1 from Combes et al. (2011, 2013) are at the lower envelope of the data distribution in the L'_{CO} vs. L_{FIR} diagram. This might suggest a poor gas content compared with star forming ULIRGs of similar L_{FIR} . It is however possible that this effect is a consequence of a substantial contribution of the AGN to the L_{FIR} , since all of them have $L_{\text{IR}} > 2 \times 10^{12} L_{\odot}$, above the turning point identified by Nardini et al. (2010).

5. Conclusions

- We present the results of CO(1-0) spectroscopic observations of 4 SDSS QSO2 at $z \sim 0.3$ observed with the 30m IRAM telescope. These QSO2 have infrared luminosities in the ULIRG regime, expanding our previous work on less infrared luminous QSO2 at $z \sim 0.3$ into this regime. The 4 QSO2 have $L_{\text{FIR}} \sim (1.2-2.5) \times 10^{12} L_{\odot}$. We have also added 9 ULIRG QSO2 at $z \sim 0.3$ -0.9 from Combes et al. (2011, 2013), which have $L_{\text{FIR}} \sim (0.2-2.5) \times 10^{13} L_{\odot}$.
- CO(1-0) detection is confirmed in one of the 4 objects observed by us: SDSS J1543-01. L'_{CO} and M_{H_2} are $(1.2 \pm 0.2) \times 10^9$ K km s $^{-1}$ pc 2 and $(9.6 \pm 1.6) \times 10^9 M_{\odot}$, respectively. The line has $\text{FWHM} = 575 \pm 102$ km s $^{-1}$. No CO(1-0) emission is detected in SDSS J0903+02, SDSS J1337-01, SDSS J1520-01. 3σ upper limits on $M(H_2)$ are 9.6, 4.3 and $5.4 \times 10^9 M_{\odot}$ respectively.
- The L'_{CO} (measurements and upper limits) of all 13 ULIRG QSO2 at $z < 1$ fall in the L'_{CO} vs. L_{FIR} and L'_{CO} vs. z correlations defined by QSO1 and QSO2 with different z and L_{IR} . They overlap as well with $z < 1$ star forming ULIRGs. Several QSO1 and QSO2 in Combes et al. (2011, 2013) mark the lower envelope defined by the scatter of the correlation. They might be gas poor objects. Alternatively, this result might be an effect of a significant contribution of the AGN to the L_{FIR} .

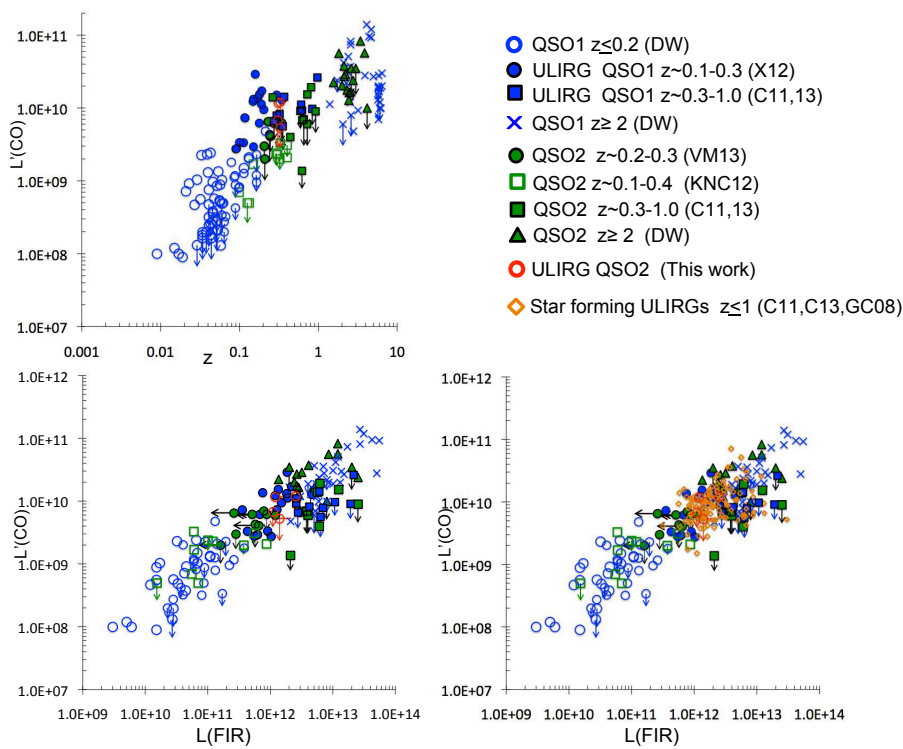


Fig. 2. L'_{CO} vs. z (top) and L'_{CO} vs. L_{FIR} (bottom) for QSO1 (blue symbols) and QSO2 (green symbols). Our 4 ULIRG QSO2 are the red open circles. References are as follows: green solid circles: QSO2 from VM13. Open green squares: QSO2 from KNC12. Green solid squares: QSO2 from C11 and C13. Green solid triangles: $z \geq 2$ QSO2 from different works (DW) (Aravena et al. 2008; Martínez Sansigre et al. 2009; Yan et al. 2010; Polleta et al. 2011; Lacy et al. 2011) // Blue crosses: $z \geq 2$ QSO1 from different works (DW) (Cox et al. 2002; Carilli et al. 2002; Walter et al. 2004; Krips et al. 2005; Riechers, Walter & Carilli 2006; Gao et al. 2007; Maiolino et al. 2007; Coppin et al. 2008; Wang et al. 2010, 2011; Riechers, Walter & Frank 2009; Riechers et al. 2009, 2006). Blue solid squares: QSO1 from C11 and C13. Open blue circles: $z \leq 0.2$ QSO1 from different works (DW) (Evans et al. 2001, 2006; Scoville et al. 2003; Pott et al. 2006; Bertram et al. 2007). Filled blue circles: ULIRG QSO1 from Xia et al. 2012 (X12). Orange small diamonds: star forming ULIRGs at $z \leq 1$ (C11, C13; Graciá Carpio et al. 2008 (GC08))

References

- Aravena M., Bertoldi F., Schinnerer E., et al. 2008, A&A, 4191, 173
 55
 Bertram T., Eckart A., Fischer S., Zuther J., Straubmeier C., Wisotzki L., Krips M., 2007, A&A, 470, 571
 Carilli C., Kohn K., Kawabe R., et al. 2002, AJ, 123, 1838
 Combes, F., García-Burillo, S., Braine, J., Schinnerer, E., Walter, F., Colina, L., 2011, A&A, 528A, 124
 Combes, F., García-Burillo, S., Braine, J., Schinnerer, E., Walter, F., & Colina, L., 2013, A&A, 550A, 41
 Coppin K., Swinbank A. M., Neri R., et al. 2008, MNRAS, 389, 45
 Cox P., Omont A., Djorgovski S. G., et al. 2002, A&A, 387, 406
 Downes, D. & Solomon, P. M., 1998, ApJ, 507, 615
 Evans A. S., Frayer D. T., Surace J. A., Sanders D. B., 2001, AJ, 121, 1893
 Evans A. S., Solomon P. M., Tacconi L., Vavilkin T., Downes D., 2006, AJ, 132, 2398
 Gao Y., Carilli C., Solomon P., Vanden Bout P., 2007, ApJ, 660, 93
 Graciá Carpio J., García-Burillo S., Planesas P., Fuente A., Usero A., 2008, A&A, 479, 703
 Guilleaume S., & Forveille T., 1989,
Grenoble Image and Line Data Analysis System (GILDAS),
 IRAM, <http://www.iram.fr/IRAMFR/GILDAS>
 Krips M., Eckart A., Neri R. et al. 2005, A&A, 439, 75
 Krips M., Neri R., Cox P., 2102, ApJ, 753, 135 (KNC12)
 Lacy, M., Sajina, A., Petric, A. O., et al., 2007, ApJ, 669L, 61
 Lacy M., Petric A., Martínez-Sansigre A., Ridgway S., Sajina A., Urrutia T., Farrah D., 2011, AJ, 142, 196 24
 Maiolino R., Neri R., Beelen A., et al. 2007, A&A, 472, L33
 Martínez-Sansigre, A., Rawlings, S., Garn, T., et al. 2006, MNRAS, 373L, 80
 Martínez Sansigre A., Karim A., Schinnerer E. et al., 2009, ApJ, 706, 184
 Nardini, E., Risaliti, G., Watabe, Y., Salvati, M., & Sani, E., 2010, MNRAS, 405, 2505
 Papadopoulos P., van der Werf P., Xilouris E., Isaak K., Gao Y., 2012, ApJ, 751, 10
 Pier, E. A., & Krolik, J. H., 1992, ApJ, 401, 99
 Polletta M., Nesvadba N., Neri R., Omont A., Berta S., Bergeron J., 2011, A&A, 533, 20
 Pott, J.-U., Eckart, A., Krips, M., Tacconi-Garman, L. E., & Lindt, E., 2006, A&A, 456, 505
 Riechers D., Walter F., Carilli C. et al. 2006, ApJ, 650, 604
 Riechers D., Walter F., Carilli C., Lewis G., 2009, ApJ, 690, 485
 Riechers D., Walter F., Frank B., 2009, ApJ, 703, 1338
 Sanders, D. B., & Mirabel, I. F., 1996, ARA&A, 34, 749
 Scoville N., Frayer D., Schinnerer E., Christopher M., 2003, ApJ, 585, L105 22
 Szokoly, G. P.; Bergeron, J.; Hasinger, G., et al., 2004, ApJS, 155, 271
 Villar Martín M., Cabrera Lavers A., Bessiere P., Tadhunter C., Rose M., de Breuck C., 2012, MNRAS, 423, 80 [VM13]
 Villar Martín M., Rodríguez M., Drouart G. et al. 2013, MNRAS, 434, 978
 Walter F., Carilli C., Bertoldi F. et al. 2004, ApJ, 615, L17
 Wang R., Carilli C., Neri R., et al. 2010, ApJ, 714, 699
 Wang R., Wagg J., Carilli C. L. et al. 2011, AJ, 142, 101
 Wu Y. et al., 2010, ApJ, 723, 895
 Xia, X. Y., Gao, Y., Hao, C.-N., et al. 2012, ApJ, 750, 92
 Yan L., Tacconi L., Fiolet N., Sajina A., Omont A., Lutz D., Zamojski M., Neri R., Cox P., Dasyra K., 2010, ApJ, 714, 100 55
 York D. G., Adelman J., Anderson S. et al., 2000, AJ, 120, 1579
 Zakamska N., Strauss M., Krolik J. et al. 2003, AJ, 126, 2125
 Zakamska N., Strauss M., Heckman, T. et al. 2004, AJ, 128, 1002